Journal of Hazardous Materials 176 (2010) 402–413

Contents lists available at ScienceDirect

Journal of Hazardous Materials

journal homepage: www.elsevier.com/locate/jhazmat

A mechanistic kinetic model for phenol degradation by the Fenton process

Ricardo F.F. Pontes[a], José E.F. Moraes[b,d], Amilcar Machulek Jr.[c,d], José M. Pinto[a,*]

[a] Chemical Engineering Department, Universidade de São Paulo, Av. Prof. Luciano Gualberto, Travessa 3, 380, 05508-900, São Paulo, SP, Brazil
[b] Escola Paulista de Engenharia Química, Universidade Federal de São Paulo, R. Arthur Ridel, 275, 09972-270, Diadema, SP, Brazil
[c] Departamento de Química, Universidade Federal de Mato Grosso do Sul, 79070-900, Campo Grande, MS, Brazil
[d] Centro de Capacitação e Pesquisa em Meio Ambiente (CEPEMA – USP), Av. Cônego Domênico Rangoni, km 270+3, 11573-000, Cubatão, SP, Brazil

ARTICLE INFO

Article history:
Received 16 June 2009
Received in revised form 6 November 2009
Accepted 9 November 2009
Available online 13 November 2009

Keywords:
Fenton process
Mathematical modeling
Parameter estimation
Wastewater treatment

ABSTRACT

The objective of this paper is to develop and validate a mechanistic model for the degradation of phenol by the Fenton process. Experiments were performed in semi-batch operation, in which phenol, catechol and hydroquinone concentrations were measured. Using the methodology described in Pontes and Pinto [R.F.F. Pontes, J.M. Pinto, Analysis of integrated kinetic and flow models for anaerobic digesters, Chemical Engineering Journal 122 (1–2) (2006) 65–80], a stoichiometric model was first developed, with 53 reactions and 26 compounds, followed by the corresponding kinetic model. Sensitivity analysis was performed to determine the most influential kinetic parameters of the model that were estimated with the obtained experimental results. The adjusted model was used to analyze the impact of the initial concentration and flow rate of reactants on the efficiency of the Fenton process to degrade phenol. Moreover, the model was applied to evaluate the treatment cost of wastewater contaminated with phenol in order to meet environmental standards.

1. Introduction

Biological processes are frequently used for the treatment of wastewaters containing organic compounds, but their application is not always viable. The presence of toxic compounds, such as phenol and benzene among other aromatic compounds that are present in many industrial effluents, may undermine the operation of the biological process. Therefore, there is a growing urge for studying and implementing alternative treatments for industrial wastewaters containing highly toxic compounds.

Advanced oxidation processes (AOPs) have appeared in recent decades as a viable alternative for the treatment of effluents containing very toxic organic compounds. Esplugas et al. [5] define AOPs as processes whose oxidation aqueous phase is based on intermediate reactions in which the hydroxyl radical ($HO^{\bullet}$) is present. These processes are able to degrade a large number of organic compounds by reduction–oxidation and free-radical reactions to carbon dioxide (CO_2) and water (H_2O). Legrini et al. [1], Gogate and Pandit [2], Pera-Titus et al. [3], Machulek et al. [4] cite among the AOPs the ones that use ozone (O_3), ultra-violet radiation (UV), ozone combined with UV, ozone with hydrogen peroxide (H_2O_2), hydrogen peroxide with UV, ozone and hydrogen peroxide with UV, as well as Fenton and photo-Fenton processes.

The main disadvantage of AOPs is the high cost of reactants, such as ozone and hydrogen peroxide, and even the operation and maintenance of special light sources such as ultra-violet lamps ([3,5,6]), in the case of photochemical AOPs.

The main advantage of the Fenton process over other AOPs is the reduced use of oxidizing agents, such as hydrogen peroxide. However, Rios-Enriquez et al. [7] mention that the presence of Fe^{2+} and Fe^{3+} requires catalyst recovery, which increases the operating costs and generate inorganic pollutants in the treated effluent.

For industrial applications, it is very important to obtain a consistent mathematical model that predicts process performance. Unfortunately, this is very challenging in the case of AOPs, because the process encompasses several chemical reactions, which would require the determination of the respective reaction rates in a mechanistic model. As a simplifying alternative to this problem, previous works have presented empirical mathematical modeling techniques, such as artificial neural networks and response surface techniques ([8–10]). In spite of the success obtained, these methodologies are very limited in comparison with phenomenological modeling, mainly for extrapolation purposes such as design and process optimization as well as scale-up studies.

In the case of the Fenton process, there are a few works that use specific phenomenological models for the degradation of a given compound. However, as expected, there are common reaction pathways for different contaminating compounds. Kang et al. [11] describe the degradation of chlorophenols by the Fenton process and use the same model structure for the degradation of phenol. Kusic et al. [12] describe a model for the degradation of

* Corresponding author. Present address: Praxair Inc., 39 Old Ridgebury Rd., Danbury CT 06810, USA. Tel.: +1 203 837 2391.
E-mail address: Jose_M_Pinto@praxair.com (J.M. Pinto).

0304-3894/$ – see front matter © 2009 Elsevier B.V. All rights reserved.
doi:10.1016/j.jhazmat.2009.11.044

phenol by the photo-Fenton process. Andreozzi et al. [13] describe the degradation of benzothiazole by the photo-Fenton process.

The objective of this paper is to develop and validate a phenomenological model that describes the reactions involved in the degradation of phenol by the Fenton process and how fast these reactions occur. The methodology presented in Pontes and Pinto [14] is applied to the current work. First, a stoichiometric model is developed to describe the reactions involved in the phenol degradation by the Fenton process, and then the kinetic model is developed to determine how fast these reactions take place. Kinetic parameter estimation is made to adjust the simulated results to the experimental data.

The structure of this paper is as follows. In Section 2, the experimental part is described and the experimental results are presented. In Section 3, a detailed study of the phenol degradation by the Fenton process is presented along with the stoichiometric model, which yields a kinetic model. In Section 4, the kinetic model is simulated and the results are compared with experimental data. A parameter sensitivity analysis is performed to determine the most influential reactions on the model. In Section 5, a kinetic parameter optimization, based on the results of the sensitivity analysis, is done to best fit the model to the experimental data. An analysis of the impact of the reactants concentration on the efficiency of phenol degradation by Fenton process as well as the treatment cost to meet environmental standards are done in Section 6. Finally, Section 7 presents the conclusions of the work.

2. Experimental work

2.1. Materials

In order to perform all experiments, the following chemical reactants were used: heptahydrated iron (II) sulfate – Merck (98%); hydrogen peroxide – Merck (30%); sulfuric acid – Synth (98%); sodium hydroxide – Sigma Aldrich (99%); phenol – Sigma Aldrich (99%); catechol – Sigma Aldrich (99%); hydroquinone – Sigma Aldrich (99%); resorcinol – Sigma Aldrich (99%) and pyrogallol – Sigma Aldrich (99%). The phenol solutions were prepared by direct dissolution of the desired phenol amount in water.

2.2. Experimental setup

Three experiments in fed-batch operation were performed in order to monitor phenol degradation by the Fenton process during 2 h. Table 1 presents the initial concentrations of iron (II) sulfate ($S_{Fe_{2+},0}$), phenol ($S_{Phenol,0}$), feed flow rates of hydrogen peroxide ($F_{H_2O_2}$) and operating conditions for each performed experiment. Note that the amount of H_2O_2 used varies in each experiment.

The following equipment was used:

- Varian Spectrophotometer. The samples were placed in quartz cells with optical path equal to 1.00 cm.
- HPLC-UFLC/Prominence from Shimadzu with UV–vis (190–700 nm) detector.

Table 1
Experimental conditions.

Parameter	Experiment A	Experiment B	Experiment C
$S_{Fe_{2+},0}$	1.0×10^{-3} mol L^{-1}	1.0×10^{-3} mol L^{-1}	1.0×10^{-3} mol L^{-1}
$F_{H_2O_2}$	0.075 mol/30 min	0.150 mol/30 min	0.300 mol/30 min
$S_{Phenol,0}$	12.1×10^{-3} mol L^{-1}	12.1×10^{-3} mol L^{-1}	12.1×10^{-3} mol L^{-1}
Temperature	30 °C		
pH	3.0		
Reactor volume	3 L		

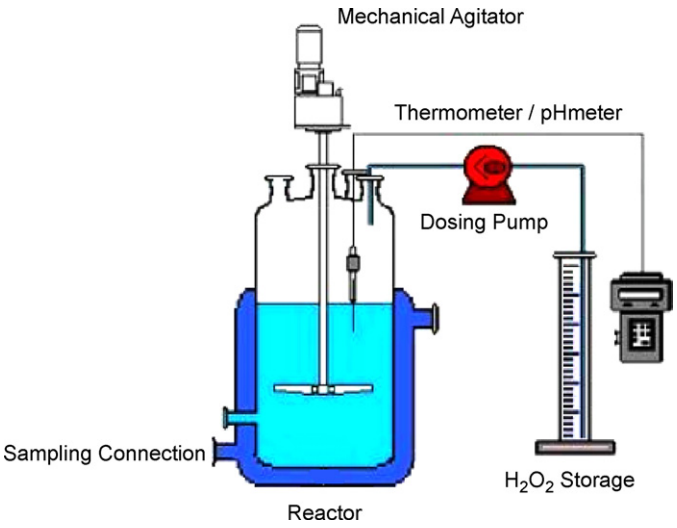

Fig. 1. Experimental setup for phenol degradation by the Fenton process.

The reactor used in the experiments was made of borosilicate glass equipped with mechanical agitator. Fig. 1 shows the setup used for the Fenton process phenol degradation experiments.

2.3. Experimental procedure

The solution temperature was controlled at 30 ± 2 °C using thermostatic bath. The pH of the synthetic solution was initially adjusted to 3.0 and maintained at that value during the experiments by the addition of concentrated sulfuric acid (H_2SO_4) and/or sodium hydroxide solution (NaOH). The Fenton reaction was then initiated by the addition of a 100 mL aqueous solution of $FeSO_4{\cdot}7H_2O$ 0.001 mol L^{-1}, followed by the addition of a determined quantity of a H_2O_2 6 mol L^{-1} solution, as shown in Table 1, for 30 min.

Duplicate samples, a solution of 5 mL each, were taken, in appropriate time intervals, for analysis during the reaction time. NaOH 10 mol L^{-1} (2 drops) was added to all samples to interrupt the reaction. Later, the samples were filtered (0.22 μm Millipore Durapore membrane) to remove the precipitated iron species, diluted and immediately analyzed by high performance liquid chromatography (HPLC).

Phenol, catechol and hydroquinone were identified and quantified by high performance liquid chromatography (UFLC chromatographer, Shimadzu) using standard compounds for comparison. A reverse phase C18 Shim-pack column (5 μm; 4.6 × 150 mm) with detection in 254 nm was used to determine the intermediate aromatic compounds, along with a Shimadzu UV–vis detector.

2.4. Experimental results

Table 2 presents the concentrations of phenol, catechol and hydroquinone at different time points for Experiments A to C.

3. Stoichiometric and kinetic models of the Fenton process

Following the methodology presented by Pontes and Pinto [14], the first step is to determine the stoichiometric model for the degradation of the contaminants present in the effluent. This model describes the chemical reactions that the contaminants undergo in the treatment. Thereafter, the kinetic model is developed that determines how fast the reactions occur and consequently how fast the compounds involved in the process are formed and consumed.

Table 2
Phenol, catechol and hydroquinone concentrations in Experiments A to C (concentrations in mmol L^{-1}).

Time (min)	Experiment A			Experiment B			Experiment C		
	S_{phenol}	$S_{catechol}$	$S_{hydroquinone}$	S_{phenol}	$S_{catechol}$	$S_{hydroquinone}$	S_{phenol}	$S_{catechol}$	$S_{hydroquinone}$
0	12.1	0.00	0.00	12.1	0.00	0.00	12.1	0.00	0.00
5	8.86	1.40	0.59	6.81	1.16	0.82	2.71	2.50	1.95
10	6.04	1.93	1.16	3.01	1.50	2.75	0.60	0.82	6.39
20	3.55	2.34	2.26	0.70	0.65	5.67	0.00	0.00	4.19
30	1.12	1.73	3.92	0.00	0.00	5.00	0.00	0.00	3.33
45	0.754	1.58	3.87	0.00	0.00	4.46	0.00	0.00	0.85
60	0.766	1.65	4.48	0.00	0.00	4.44	0.00	0.00	0.74
75	0.774	1.67	4.38	0.00	0.00	4.34	0.00	0.00	0.70
90	0.767	1.66	4.27	0.00	0.00	4.14	0.00	0.00	0.63
120	0.772	1.68	4.25	0.00	0.00	4.09	0.00	0.00	0.57

3.1. Notation

The process is modeled as a system of j compounds that undergo a set of n chemical reactions.

The phenol degradation by Fenton process model contains the following variables and parameters:

$\nu_{j,n}$	stoichiometric coefficient for compound j in reaction n (dimensionless)
C_{tr}	treatment cost (US$/1000 m^3 of wastewater)
$F_{H_2O_2}$	hydrogen peroxide stream flow rate (mol min^{-1})
k_n	kinetic parameter for reaction n (L mol^{-1} s^{-1}, except where otherwise indicated)
r_n	rate of reaction n (mol L^{-1} s^{-1})
R_j	compound j consumption/production rate (mol L^{-1} s^{-1})
S_j	molar concentration for compound j (mol L^{-1})
$S_{j,0}$	initial molar concentration for compound j (mol L^{-1})
$S_{j,f}$	final molar concentration for compound j (mol L^{-1})
$S_{j,f,b}$	final molar concentration for compound j (mol L^{-1}) for the simulation with kinetic parameters from the literature

3.2. Stoichiometric model

The stoichiometric model describes which reactions take place in the Fenton process. Note that a simplistic stoichiometry may not describe accurately the Fenton process, whereas one that is too complex may result in a large number of kinetic parameters that would not be obtainable.

The original Fenton reaction was developed by H. Fenton. In the presence of an iron (II) salt, hydrogen peroxide is dissociated, yielding the hydroxyl radical. Andreozzi et al. [13], Hislop and Bolton [15], and Pignatello et al. [16] describe the Fenton reaction by:

$$Fe^{2+} + H_2O_2 \rightarrow Fe^{3+} + HO^{\bullet} + OH^{-}$$

[2] and Kim and Vogelpohl [17] proposed a structure for the photo-Fenton process that can be simplified to the structure to the Fenton process presented in Fig. 2.

In the absence of UV radiation, such as the Fenton process, the reduction for Fe^{3+} reaction – and the velocity limiting reaction of the Fenton process – is ([11,16,18]):

$$Fe^{3+} + H_2O_2 \rightarrow Fe^{2+} + H^{+} + HO_2^{\bullet}$$

The stoichiometric model used in this paper is based on the one described by Kang et al. [11]. However, it takes into account the formation of ortho and para isomers in the oxidation of phenol. The oxidation of phenol in the meta position was neglected, since according to Alnaizy and Akgerman [19], the formation of resorcinol is about 1000 lower than the formation of catechol (*ortho*-oxidation) and hydroquinone (*para*-oxidation). These reactions are given in Table 3 along with their rate constants.

With respect to Fig. 2, reactions 1 through 3 represent stage 1, reaction 4 represents stage 2, reactions 5 through 21 represent stage 4, and reactions 22 through 48 represent stage 3. More specifically, reactions 39 to 48 represent the degradation of the aliphatic compounds.

The following hypotheses were made:

- all the reactions are irreversible except for R10, R28, R29, R32 and R33′, as established by Kang et al. [11].;
- all the kinetic constants listed in Table 3 are based on a solution with pH 3.0;
- the pH of the reaction medium remains constant during the experiments;
- constant volume of reaction because of the low concentration of reactants and products;
- isothermal reaction medium.

The stoichiometric model for the phenol degradation by Fenton process has 53 reactions and 26 compounds. Phenol, 1,2 and 4-DHCD•, Catechol, Hydroquinone, THB, 1,2 and 4-Semiquinone•, 1,2 and 4-Benzoquinone and THCD• are the aromatic compounds, whereas muconic, maleic and oxalic acid, as well as their radicals, are the aliphatic compounds. Hence, the following concentration variables are defined:

$$S_{arom} = \sum_{j \in \{aromatic\}} S_j \quad (1)$$

$$S_{aliph} = \sum_{j \in \{aliphatic\}} S_j \quad (2)$$

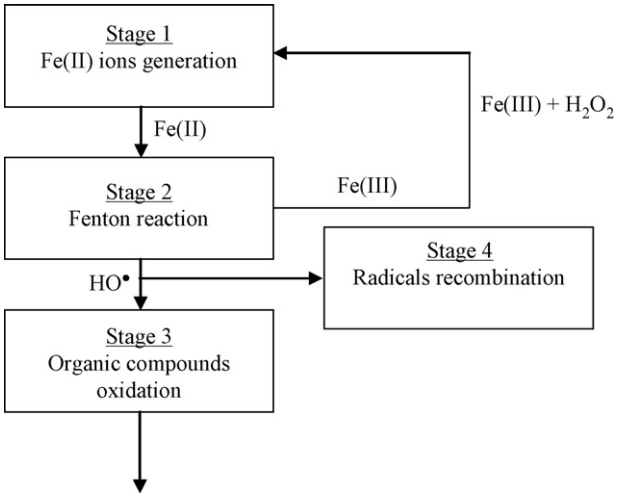

Fig. 2. Structure of the phenol degradation by the Fenton process.

Table 3
Stoichiometric model for the phenol degradation by the Fenton process.

Reaction	k_r	Ref	Reaction	k_r	Ref
(R1) $Fe^{3+} + H_2O_2 \rightarrow Fe^{2+} + H^+ + HO_2^\bullet$	1.0×10^{-2}	(a)	(R25) 1,4-DHCD$^\bullet$ + $Fe^{3+} \rightarrow Fe^{2+}$ + Hydroquinone	7.0×10^{3}	(a)
(R2) $Fe^{3+} + HO_2^\bullet \rightarrow Fe^{2+} + H^+ + O_2$	3.3×10^{5}	(b)	(R26) 1,2-DHCD$^\bullet$ + HO$^\bullet$ → THB	2.0×10^{10}	(a)
(R3) $Fe^{3+} + O_2^{\bullet-} \rightarrow Fe^{2+} + O_2$	5.0×10^{7}	(a, b)	(R27) 1,4-DHCD$^\bullet$ + HO$^\bullet$ → THB	2.0×10^{10}	(a)
(R4) $Fe^{2+} + H_2O_2 \rightarrow Fe^{3+} + HO^\bullet \rightarrow OH^-$	6.3×10^{1}	(a, b)	(R28) Catechol + $Fe^{3+} \rightleftarrows$ 1,2-Semiquinone$^\bullet$ + Fe^{2+} + H^+	1.0×10^{0}	(a)
				2.4×10^{1}	(a)
(R5) $HO^\bullet + H_2O_2 \rightarrow HO_2^\bullet + H_2O$	3.3×10^{7}	(b)	(R29) Hydroquinone + $Fe^{3+} \rightleftarrows$ 1,4-Semiquinone$^\bullet$ + Fe^{2+} + H^+	1.0×10^{0}	(a)
				2.4×10^{1}	(a)
(R6) $HO_2^\bullet + H_2O_2 \rightarrow HO^\bullet + H_2O + O_2$	5.0×10^{-1}	(c)	(R30) Catechol + HO$^\bullet$ → THCD$^\bullet$	1.1×10^{10}	(d)
(R7) $2HO_2^\bullet \rightarrow H_2O_2 + O_2$	8.3×10^{5}	(a–c)	(R31) Hydroquinone + HO$^\bullet$ → THCD$^\bullet$	5.2×10^{9}	(d)
(R8) $HO_2^\bullet + HO^\bullet \rightarrow H_2O + O_2$	1.0×10^{10}	(a, b)	(R32) 1,2-Semiquinone$^\bullet$ + Fe^{2+} + $H^+ \rightleftarrows$ 1,2-Benzoquinone + Fe^{3+}	1.0×10^{3}	(a)
				1.1×10^{1}	(a)
(R9) $Fe^{2+} + HO^\bullet \rightarrow Fe^{3+} + OH^-$	3.2×10^{8}	(a, b)	(R33) 1,4-Semiquinone$^\bullet$ + Fe^{2+} + $H^+ \rightleftarrows$ 1,4-Benzoquinone + Fe^{3+}	1.0×10^{3}	(a)
				1.1×10^{1}	(a)
(R10) $HO_2^\bullet \leftrightarrow H^+ + O_2^{\bullet-}$	1.6×10^{5} s^{-1}	(a, b)	(R34) THCD$^\bullet$ + $Fe^{3+} \rightarrow$ THB + Fe^{2+} + H^+	7.0×10^{3}	(a)
	1.0×10^{10}	(a, b)			
(R11) $Fe^{2+} + HO_2^\bullet + H^+ \rightarrow Fe^{3+} + H_2O_2$	1.2×10^{6}	(a, b)	(R35) Fe^{3+} + THB → Fe^{3+} + AML	1.0×10^{1}	(a)
(R12) $Fe^{2+} + 2H^+ + O_2^{\bullet-} \rightarrow Fe^{3+} + H_2O_2$	1.0×10^{7}	(a, b)	(R36) 1,2-Benzoquinone + HO$^\bullet$ → MA$^\bullet$	1.2×10^{9}	(a)
(R13) $2HO^\bullet \rightarrow H_2O_2$	4.2×10^{9}	(a)	(R37) 1,4-Benzoquinone + HO$^\bullet$ → MA$^\bullet$	1.2×10^{9}	(a)
(R14) $HO^\bullet + O_2^{\bullet-} \rightarrow OH^- + O_2$	1.0×10^{10}	(a, b)	(R38) THB + HO$^\bullet$ → AML	4.0×10^{10}	(a)
(R15) $HO_2^\bullet + O_2^{\bullet-} + H^+ \rightarrow H_2O_2 + O_2$	9.7×10^{7}	(a)	(R39) MA + HO$^\bullet$ → MA$^\bullet$	5.0×10^{8}	(a)
(R16) $SO_4^{2-} + HO^\bullet + H^+ \rightarrow H_2O + SO_4^{\bullet-}$	1.2×10^{6}	(a)	(R40) AML + HO$^\bullet$ → AML$^\bullet$	6.0×10^{9}	(d)
(R17) $SO_4^{\bullet-} + OH^- \rightarrow SO_4^{2-} + HO^\bullet$	1.0×10^{7}	(e)	(R41) AOX + HO$^\bullet$ → AOX$^\bullet$	1.4×10^{6}	(d)
(R18) $SO_4^{\bullet-} + H_2O_2 \rightarrow H^+ + HO_2^\bullet + SO_4^{2-}$	3.0×10^{8}	(e)	(R42) Fe^{3+} + MA$^\bullet$ → Fe^{2+} + MA	1.0×10^{1}	(a)
(R19) $SO_4^{\bullet-} + HO_2^\bullet \rightarrow H^+ + O_2 + SO_4^{2-}$	6.6×10^{2}	(e)	(R43) Fe^{3+} + AML$^\bullet$ → Fe^{2+} + AML	1.0×10^{1}	(a)
(R20) $SO_4^{\bullet-} + Fe^{2+} \rightarrow Fe^{3+} + SO_4^{2-}$	5.0×10^{8}	(e)	(R44) Fe^{3+} + AOX$^\bullet$ → Fe^{2+} + AOX	1.0×10^{1}	(a)
(R21) $SO_4^{\bullet-} + H_2O \rightarrow H^+ + HO^\bullet + SO_4^{2-}$	6.0×10^{9}	(e)	(R45) MA + HO$^\bullet$ → AML + CO_2	5.0×10^{8}	(a)
(R22) HO$^\bullet$ + Phenol → 1,2-DHCD$^\bullet$	3.3×10^{9}	(a)	(R46) AML + HO$^\bullet$ → AOX + CO_2	6.0×10^{9}	(d)
(R23) HO$^\bullet$ + Phenol → 1,4-DHCD$^\bullet$	3.3×10^{9}	(a)	(R47) AOX + HO$^\bullet$ → CO_2	1.4×10^{6}	(d)
(R24) 1,2-DHCD$^\bullet$ + $Fe^{3+} \rightarrow Fe^{2+}$ + Catechol	7.0×10^{3}	(a)	(R48) Fe^{3+} + AOX → Fe(III)-organocomplexes	1.0×10^{0}	(a)

DHCD = di-hydroxy-cyclohexa-di-enyl radical; THB = tri-hydroxy-benzene; THCD = di-hydroxy-cyclohexa-di-enyl radical; MA = muconic acid; AML = fumaric/maleic acid; AOX = oxalic acid.
(a) Kang et al. [11]; (b) Andreozzi et al. [13]; (c) Alnaizy and Akgerman [19]; (d) Notre Dame Radiation Laboratory Radiation Chemistry Data Center (http://www.rcdc.nd.edu/) [20]; (e) de Laat et al. [21].

3.3. Fenton process kinetic model

The kinetic model determines how fast the reactions in the stoichiometric model take place; hence it determines the production/consumption rate R_j for each compound.

The reaction rates r_n for the reactions involved in the stoichiometric model are given by:

$$r_n = k_n . \prod_j S_j^{\nu_{j,n}} \quad \forall n \tag{3}$$

where S_j is the molar concentration of compound j and $\nu_{j,n}$ is its stoichiometric coefficient in reaction n.

Reactions (R10), (R28), (R29), (R32) and (R33) are the only reversible reactions in the model, as defined in Ref. [11], for which the reverse kinetic constants are significant. Therefore, it is necessary to also calculate the reverse reaction rates.

Therefore, for the Fenton process the production/consumption rate R_j for each compound j are:

$$R_j = \sum_n \nu_{j,n} . r_n \tag{4}$$

Previous papers such as [11,13,19] used the pseudo-steady state hypothesis for the simulation of the concentrations of inorganic radicals such as hydroxyl, peroxyl and oxyl. However, this paper does not rely on this simplification and therefore simulates their concentrations in transient state.

For batch operation, the mass balance for compound j is given by:

$$\frac{dS_j}{dt} = R_j \tag{5}$$

For semi-batch operation, where only reactant j, such as hydrogen peroxide, is added into the reactor by a feed stream, the mass balance is given by:

$$\frac{dS_{H_2O_2}}{dt} = R_{H_2O_2} + \frac{1}{V} F_{H_2O_2} \tag{6}$$

The kinetic model for the phenol degradation by a batch Fenton process has 79 algebraic and 26 differential equations, 53 kinetic parameters, 105 variables which are:

- 26 concentrations for the compounds in the reactor;
- 53 reaction rates;
- 26 compounds production/consumption rates.

In the case of semi-batch operation, the following 27 parameters have to be defined:

- 26 concentrations for the compounds in the feed stream
- 1 flow rate.

For the dynamic simulation of this model, the following definitions are needed:

- Values for the 53 kinetic parameters (k_n);
- Initial values for the 26 concentrations of the j compounds (S_j);
- Values for the 26 concentrations for the compounds in the feed stream ($S_{j,F}$)
- H_2O_2 feed stream flow rate ($F_{H_2O_2}$).

4. Simulation of the Fenton process model

4.1. Comparison between experimental data and simulated results

The simulation of the kinetic model was done using *MATLAB V7.0* with the *ODE23T* integrator ([22]) that solves systems of moderately stiff DAEs (differential algebraic equations). The three sets of experiments previously described were simulated, whose initial conditions are given in Table 1. The set of parameters relies on the literature values provided in Table 3.

Fig. 3 shows the experimental data and the simulation of the proposed model for experiments A, B and C, respectively. Moreover, the experimental data is presented in Table 2.

Although the simulation results in a relatively accurate phenol prediction, the catechol and hydroquinone predicted concentrations do not agree with the experimental data. The correlation coefficients for the simulation of the literature and estimated parameters are presented in Section 5.

4.2. Sensitivity analysis

Besides comparing the experimental results and those of the proposed model, sensitivity analysis for all the kinetic parameters used in the model was performed. The established range for all the rates was the following:

$$k_{n,\min} = 0.5k_n \leq k_n \leq 1.5k_n = k_{n,\max} \quad (7)$$

Fig. 4 shows the results of the sensitivity analysis of the most influential parameters on the phenol, catechol and hydroquinone concentration ratios ($S_{j,f}/S_{j,f,b}$), respectively, for Experiment A at the end of the simulation (t = 120 min).

As expected, the phenol oxidation kinetic parameters, k_{22} and k_{23}, are the most influential in the final concentration results, mainly for phenol. For a 50% decrease in the k_{22} and k_{23} values, there was approximately a 60% and 30% increase in the phenol final concentration, respectively. These parameters are also influential for catechol and hydroquinone, since the same decrease in the values of k_{22} and k_{23} resulted in the decrease of about 30% in the final concentration values for catechol and hydroquinone, respectively. As expected, the higher the k_{22} value with respect to k_{23}, the higher the catechol-to-hydroquinone ratio, and vice-versa.

The Fenton reaction rate, r_4, is at least 50 times larger than the phenol oxidation by hydroxyl radical reaction rates, r_{22} and r_{23}, and, therefore, is not the limiting step in the rate of the phenol degradation. The Fenton reaction kinetic constant, k_4, has a small influence on the phenol concentration, mainly during the initial phase of the degradation process. A value of 31.5 for k_4 (50% decrease in the original value) yields an increase in 10% in the phenol concentration at t = 5 min, but at t = 120 min this difference becomes negligible.

The kinetic parameters for the catechol and hydroquinone oxidation by the hydroxyl radical reactions, k_{30} and k_{31}, are also significantly influential. A 50% decrease in the k_{30} value yields an approximate 80% increase in the catechol concentration, whereas a 50% decrease in the k_{31} value yields an approximate 40% increase in the hydroquinone concentration.

For the kinetic parameters k_{38}, k_{40} and k_{46}, related to the THB and maleic acid oxidation by hydroxyl radical reactions, there was an impact of approximately 5% in the phenol, catechol and hydroquinone concentration for 50% changes in their values. Variations in the values of the DHCD radical and benzoquinones oxidation by hydroxyl radical reaction rates yielded changes in these final concentrations lower than 5%.

The oxidation of organic compounds by the iron (III) reactions displayed a lower influence, once variations of 50% in the values of k_{28}, k_{29}, k_{32}, k_{33}, k_{34}, k_{35}, k_{42}, k_{43} and k_{44} yielded 1–2% variations in the final concentrations of the three studied compounds.

Theoretically, the oxalic acid complexation reaction rate, k_{48}, influences the phenol final concentration, since it strips the iron from the reaction mean, but this effect was not detected by the analysis.

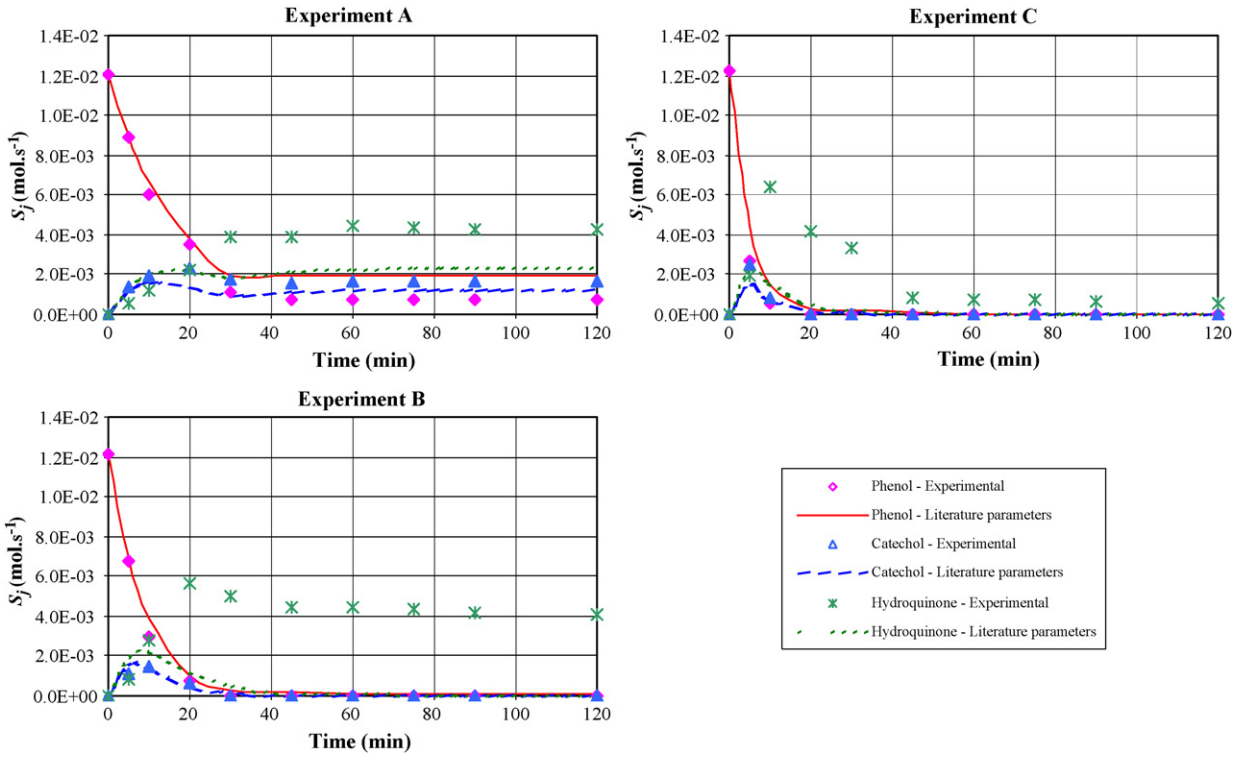

Fig. 3. Simulation of the proposed model with the parameters from Table 3 and experimental data for Experiments A, B and C.

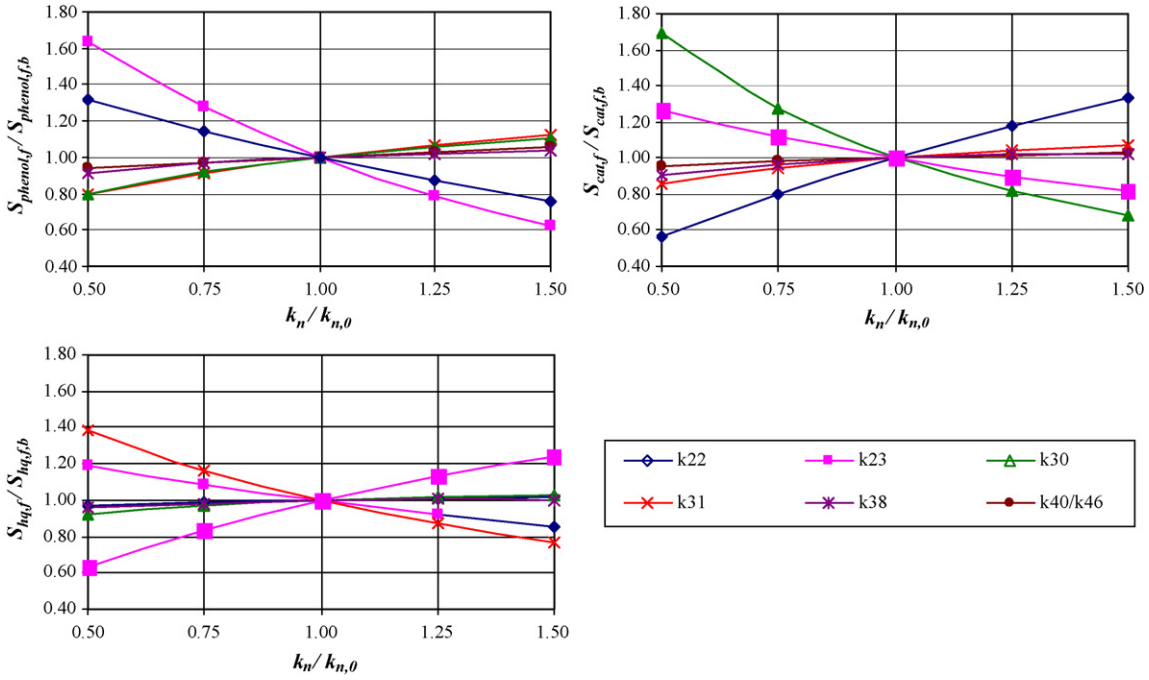

Fig. 4. Phenol, catechol and hydroquinone concentration sensitivity analysis for Experiment A at $t = 120$ min.

The remaining kinetic parameters did not have significant influence on the phenol, catechol and hydroquinone concentrations.

5. Kinetic parameter estimation

In order to find a better fit for the simulated results with the experimental data of Experiments A to C, the kinetic parameters were estimated. This adjustment was done using *MATLAB V7.0* with the sub-routine *LSQCURVEFIT* ([23]), which solves nonlinear curve-fitting problems in the least-squares sense.

The adjusted kinetic parameters were those that according to the sensitivity analysis mostly influenced the simulated results and these are listed in Table 4, as well as their variation with regard to the original value.

Table 4
Adjustment of the kinetic parameters.

Parameter	Original value ($L\,mol^{-1}\,s^{-1}$)	Adjusted value ($L\,mol^{-1}\,s^{-1}$)	Variation (%)
k_{22}	3.3×10^9	1.0×10^{10}	212
k_{23}	3.3×10^9	7.7×10^9	133
k_{24}	7.0×10^3	7.0×10^3	0
k_{25}	7.0×10^3	4.2×10^3	−40
k_{26}	2.0×10^{10}	2.1×10^{10}	3
k_{27}	2.0×10^{10}	2.3×10^{10}	15
k_{28}	1.0×10^0	4.4×10^{-1}	−56
k_{29}	1.0×10^0	8.0×10^{-2}	−99
k_{28r}	2.4×10^1	4.6×10^1	93
k_{29r}	2.4×10^1	7.3×10^0	−70
k_{30}	1.1×10^{10}	2.1×10^{10}	93
k_{31}	5.2×10^9	1.5×10^9	−71
k_{34}	7.0×10^3	3.8×10^3	−46
k_{35}	1.0×10^1	4.0×10^0	−60
k_{36}	1.2×10^9	4.2×10^8	−65
k_{37}	1.2×10^9	1.0×10^9	−14
k_{38}	4.0×10^{10}	5.8×10^{10}	46
k_{40}/k_{46}	6.0×10^9	8.7×10^9	44
$k_{42}/k_{43}/k_{44}$	1.0×10^1	3.7×10^1	268
k_{48}	1.0×10^0	2.6×10^0	157

The performed adjustment estimated a larger value for parameter k_{22} than the one estimated for k_{23}, which results in a higher formation rate of catechol than of hydroquinone. The sum of these two estimated parameters results in faster phenol degradation. Some of the estimated parameters underwent considerable variations, such as the oxidation by iron (III) of hydroquinone, k_{29}, muconic, maleic and oxalic acids, k_{42} to k_{44}, as well as the complexation of iron (III) oxalate, k_{48}.

With the estimated parameters, new simulations for Experiments A to C were made. Figs. 4–6 present the results of the simulations with the adjusted parameters, those with the literature values and the experimental ones.

The adjustment for the hydroquinone concentration in Experiment C noticeably produced the most discrepant result with respect to the experimental data, partially due to the high hydroquinone peak at $t = 10$ min.

It is important to note that any relative deviation from the experimental to the simulated concentrations is more amplified for benzodiols than for phenol. For instance, in Experiment A, at $t = 5$ min, there is a relative deviation of −2.2% from the experimental to the simulated phenol concentrations, while for the catechol and hydroquinone concentrations, the relative deviations at the same time are 14.2% and 142.9%, respectively. However, in absolute terms the deviation for phenol is 0.19 mmol L^{-1}, while the absolute deviations for catechol and hydroquinone are 0.20 and 0.84 mmol L^{-1}. Therefore, the absolute variations are small compared to the initial phenol concentration of 12 mmol L^{-1}.

The estimated values for k_{22} and k_{23} may seem large with respect to the initial values, but they are still within the bounds of the wide range of the kinetic constants found in the literature for phenol oxidation by the hydroxyl radical reaction. Note that Kang et al. [11] cite a value of 6.6×10^9 L mol^{-1} s^{-1} for the kinetic constant for the oxidation of phenol by hydroxyl radical reaction whereas the Notre Dame Radiation Chemistry Data Center (NDRCDC) [20] lists a value of 1.8×10^{10} L mol^{-1} s^{-1}. In the proposed model, the summation of k_{22} and k_{23} yields a value of 1.77×10^{10} L Mol^{-1} s^{-1} that represents the overall kinetic constant for the oxidation of phenol by the hydroxyl radical (in both *ortho* and *para* positions). The

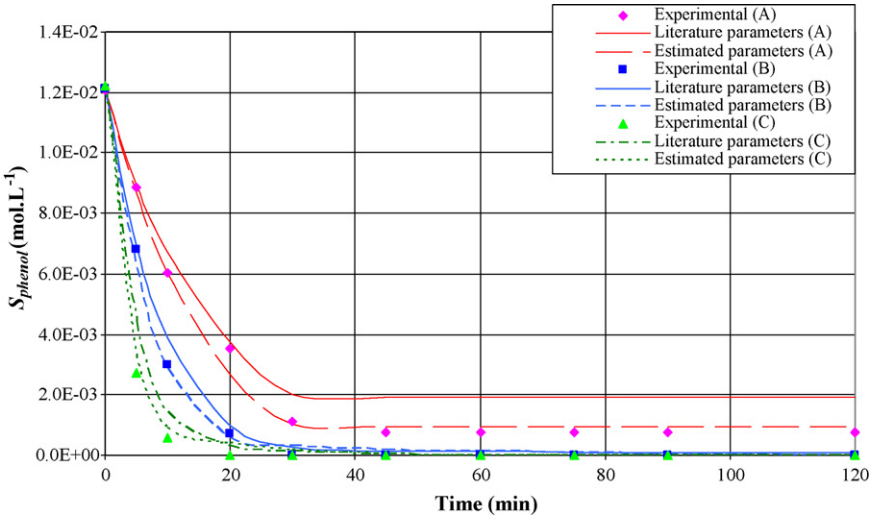

Fig. 5. Concentration profile for phenol in Experiments A, B and C.

kinetic parameters from Ref. [20] were found for pH values in the 6–7 range; hence, a large adjustment should be expected for a pH value of 3.0 as used in the experiments.

Our experimental results consistently show a larger formation of product from the *ortho*- (catechol) than from the *para*- (hydroquinone) oxidation. Similar results were reported by Alnaizy and Akgerman [19] and Lipczynska-Kochany [24]. These are parallel reactions that compete for the same reactants and therefore a higher rate constant is expected for the reaction that generates more products. The initial values for the rate constants were adjusted and a higher value was obtained for k_{22}, related to the *ortho*-oxidation of phenol, than for k_{23}, related to the *para*-oxidation reaction.

The analysis of the simulated results and the experimental data reveals that for Experiment A (Fig. 5) the reactant concentrations are not enough for the complete oxidation of the organic compounds, since there is some unreacted phenol (6% of the initial concentration). The lack of reactants yields insufficient production of the hydroxyl radical, which in turn results in relatively high residual concentrations of catechol and hydroquinone. Initially, as phenol degrades, the production rates of these two compounds are high and therefore their concentrations increase. As H_2O_2 addition ends at $t = 30$ min, the hydroxyl radical formation reactions is drastically reduced, in particular the Fenton reaction. Hence, the concentrations of aromatic compounds practically stabilize. There is a small increase in the catechol and hydroquinone concentrations after this interruption, once the oxidation of 1,2 and 1,4-DHCD$^{\bullet}$ by iron (III) goes on until most of the iron in the reaction medium is reduced to iron (II).

For Experiments B (Fig. 6) and C (Fig. 7), the H_2O_2 concentration is sufficient for the degradation of phenol and catechol, and for Experiment C, as well as for the degradation of hydroquinone. It can be noticed that even after all H_2O_2 was added, hydroxyl radical is still generated in the reaction medium. Moreover, the catechol degradation occurs first because the catechol oxidation by hydroxyl radical parameter, k_{30}, is larger than that of hydroquinone, k_{31}.

The calculated correlation coefficients for the simulation of the three experimental sets with literature and estimated parameters are given in Table 5.

The constants with the highest values are the ones related to the reactions involving the hydroxyl, peroxyl and oxyl radicals, whereas the constants with the lowest values are the ones involving the oxidation–reduction reactions of iron and organic compounds. Therefore, the difference in these values is due to the existence of several types of reactions in the Fenton process.

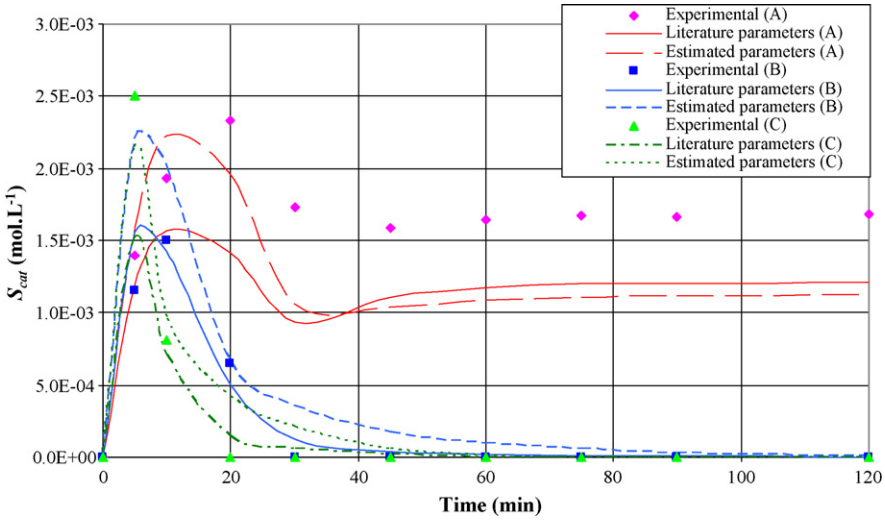

Fig. 6. Concentration profile for catechol in Experiments A, B and C.

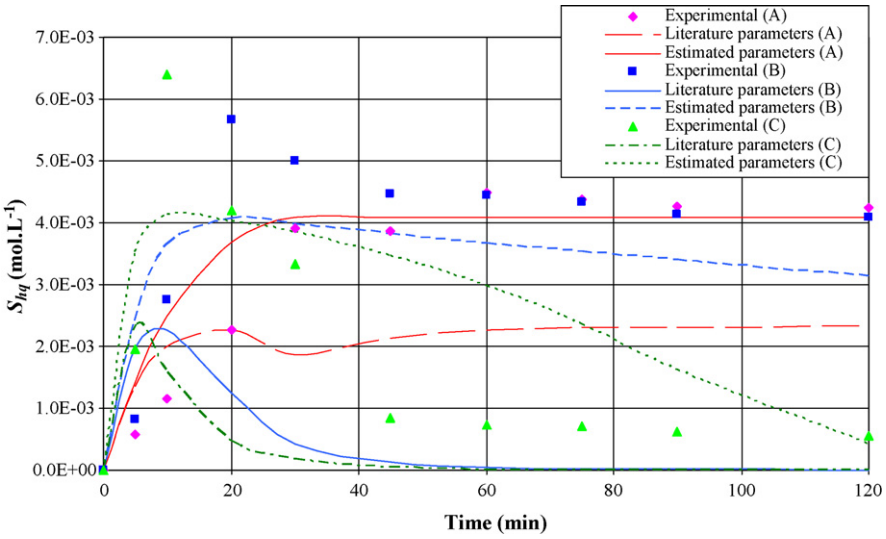

Fig. 7. Concentration profile for hydroquinone in Experiments A, B and C.

Table 5
Correlation coefficients for the simulation with literature and estimated parameters.

Experiment	Correlation coefficient (R^2)	
	Simulation with literature parameters	Simulation with estimated parameters
A	0.8326	0.9606
B	0.5595	0.9531
C	0.7457	0.8874
Global	0.7063	0.9334

Even with large constant values, the reaction rates such as r_{30} and r_{31} are not much larger than the ones involving iron species such as r_{28} and r_{29} due to the fact that the hydroxyl radical concentration is about 10^{-8} smaller than the iron (III) concentration during the batch operation.

Also, reactions that were not influential in the sensitivity analysis might exert bigger influence under different circumstances than the ones simulated.

Therefore, whereas some of the constants might be very low in relation to others, the resulting reaction rates are not necessarily negligible. Hence, the model takes into account all the reactions listed.

6. Analysis of the reactant concentrations

This section presents the effect of the concentrations of the two main reactants, iron (II) and H_2O_2 on phenol degradation by the Fenton process, by using the adjusted kinetic model. First, the concentration profiles of these reactants during the three experiments is presented, as well as a study of the H_2O_2: iron (II) ratio. Then simulations are made with different reactants ratio and batch time other than the ones used in the experiments. Finally, the cost of treating a phenol contaminated wastewater to meet *CONAMA* (Brazilian National Environmental Council) standards is evaluated and analyzed.

6.1. Simulated reactant concentrations profiles for the performed experiments

Iron (II) and H_2O_2 concentrations were simulated for the duration of the experiments with the estimated parameter values. Fig. 8 shows the results of the simulations. The H_2O_2: iron (II) molar ratios, relative to the total quantities used, for Experiments A to C are 25:1, 50:1 and 100:1. Fig. 9 shows how the ratios change as the reactants are consumed during these experiments.

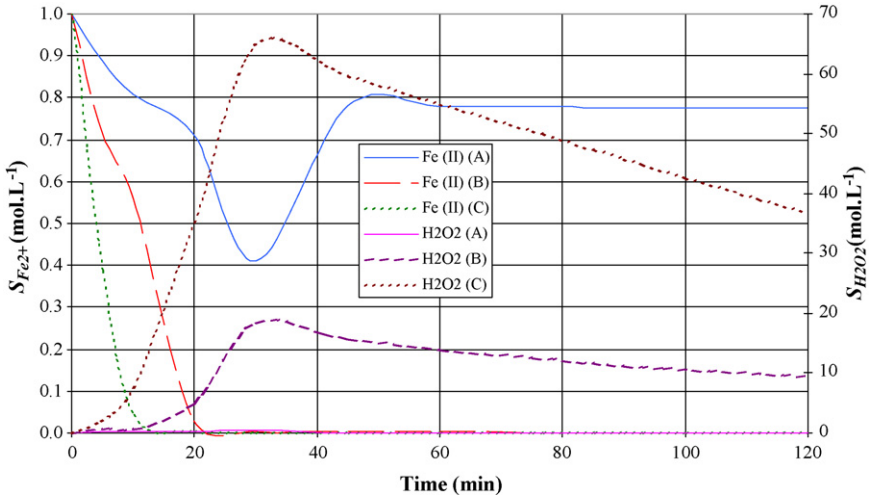

Fig. 8. Calculated concentration of iron (II) and H_2O_2 during the experiments.

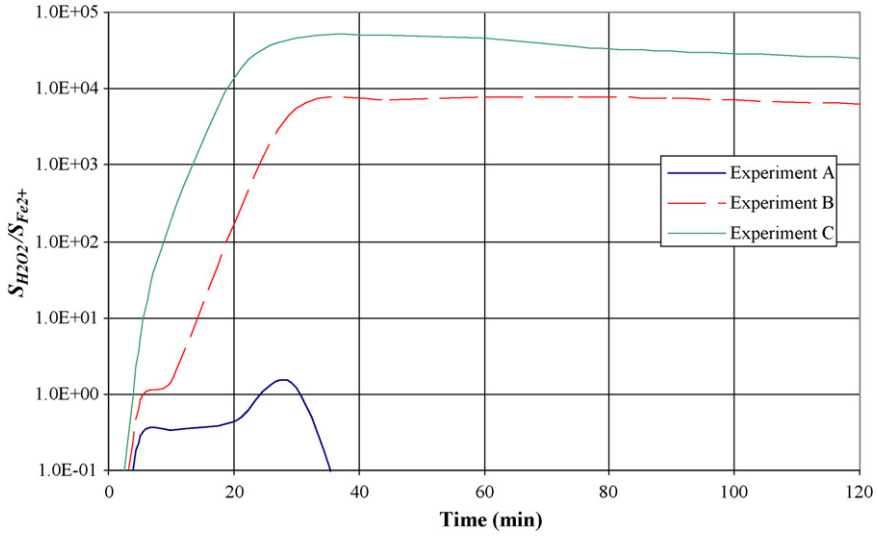

Fig. 9. Calculated H_2O_2/Iron (II) concentration ratios during the experiments.

It can be noted that in Experiment A there is a shortage of H_2O_2, since only 60% of the iron (II) was oxidized, as seen in $t = 30$ min (end of the H_2O_2 addition to the reaction medium). Thereafter, iron (II) regenerates by the oxidation of the aromatic and aliphatic compounds; however the low H_2O_2 concentration, below 1.0×10^{-3} mol L^{-1}, caused the iron (II) to become almost inactive during the reaction. In Experiments B and C, there is clearly excess of H_2O_2 in relation to iron (II); the H_2O_2 consumption is limited by the iron (II) regeneration. It can be also noted that almost all iron present in these two experiments after $t = 20$ min is in iron (III) state.

6.2. Impact of the reactant concentrations and batch time on the Fenton process efficiency

Besides the organic compounds, there are other compounds present in the reaction medium that react with the hydroxyl radical. Hydrogen peroxide as well as the iron (II) ion can function as direct scavengers of the hydroxyl radical or indirect ones by increasing the rate of formation of the peroxyl and oxyl radicals. Hence, increasing the reactants concentration does not always yield a higher organic material degradation in the Fenton process. Simulations of the mathematical model developed by this work can show this. This model can be also used to predict the optimal feed concentrations for hydrogen peroxide and iron (II) sulfate in a Fenton process reactor in continuous operation.

The simulations made for the analysis of the initial concentrations of the reactants were made using the experimental setup described in Section 3. The residual aromatic compounds concentration, S_{arom}, was evaluated at the end of each simulation, and is defined by Eqn. (1).

Simulations for different values of initial concentration of $FeSO_4$ and flow rate of H_2O_2 were performed, hence yielding different final concentration values for the aromatic compounds. Fig. 10 shows these concentrations as a function of the initial concentration of $FeSO_4$ and the H_2O_2 flow rate, respectively in log scale. The experimental points are marked with "**x**" in Fig. 10.

Fig. 10 shows that an increase in the H_2O_2 feed stream yields increased removal of the aromatic compounds in the reaction medium, as long as there is enough iron (II) to break the hydrogen peroxide into hydroxyl radical. However, Fig. 10 also shows that for $FeSO_4$, an increase in initial concentration results in an efficiency loss for the Fenton process. This efficiency loss increases in the case in which the H_2O_2 feed stream is 0.150 mol/30 min (Experiment B feed stream), once the $FeSO_4$ concentration passes 5.0×10^{-3} mol L^{-1}. For a H_2O_2 feed stream of 0.300 mol/30 min (Experiment C feed stream), the efficiency loss occurs for an initial $FeSO_4$ concentration above 20 mmol L^{-1}.

Larger batch times may also improve the Fenton process efficiency as long as there is enough H_2O_2 to maintain the degradation of the organic compounds. Fig. 11 shows the effect of the batch time on the degradation of the aromatic compounds using the same inlet H_2O_2 flow rates and initial iron (II) concentrations used in the experiments.

As shown in Fig. 8, for an initial iron (II) concentration of 1 mmol L^{-1}, a H_2O_2 flow rate of 0.075 mol/30 min is insufficient to degrade more than approximately 50% of the aromatic compounds initially present in the batch operation, which is 12.1×10^{-3} mol L^{-1}. For the conditions of Experiment C, about 94% of the aromatic compounds are degraded after 120 min. However, if the batch time is increased to 150 min, over 99% of these compounds degrade.

6.3. Cost evaluation for phenol contaminated wastewater treatment in fed-batch operation

The Brazilian Environmental Council – *CONAMA* ([25]) imposes a maximum phenol concentration value of 0.5 mg/L in wastewaters (Resolution 357/05), which is equivalent to approximately 5.32×10^{-6} mol L^{-1}. This value can be used conservatively as an upper bound to the final concentrations of all aromatic compounds, $S_{arom,f}$. For the cost evaluation study, the initial phenol concentration, $S_{phenol,0}$, was set to 12.1×10^{-3} mol L^{-1}, as used in the experiments, and it is assumed that phenol is the only aromatic compound initially present in the wastewater.

The cost evaluation developed in this section only considered reactant costs for the treatment. Table 6 presents orientative prices for the two main reactants of the Fenton process.

Table 6
Orientative prices for Fenton process reactants.

Reactant	Orientative price (US$/mol)	Source
H_2O_2	0.003	http://www.h2o2.com/
$FeSO_4$	0.036	http://www.the-innovation-group.com

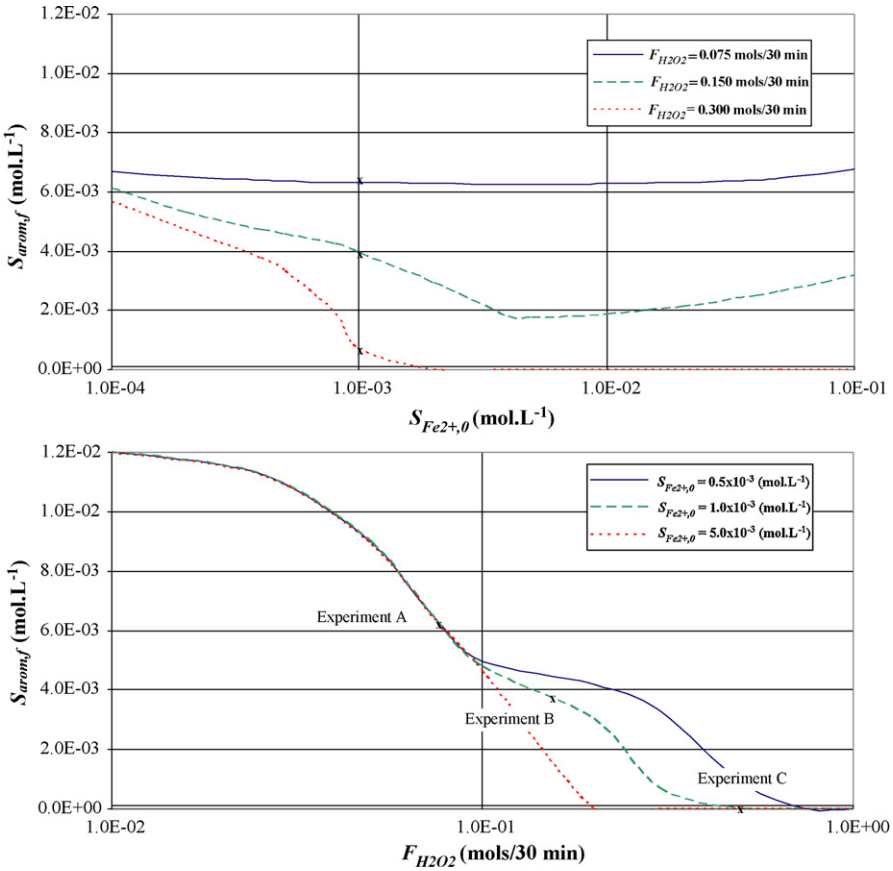

Fig. 10. Residual concentration of aromatic compounds as a function of the initial iron (II) sulfate concentration and inlet H_2O_2 flow rate.

The results presented in Fig. 10 provide the values of initial iron (II) concentrations and H_2O_2 flow rates that yield a residual aromatic compounds concentration equal to the *CONAMA* upper bound.

Six cases are studied for cost evaluation. In Cases I to III, the initial iron (II) concentration is fixed and the H_2O_2 flow rate is varied, and for each case the corresponding final aromatic compound concentration is calculated. Table 7 lists the three initial iron (II) concentrations (Cases I to III) for each case and the corresponding stoichiometric H_2O_2 flow rate to reach the *CONAMA* requirement, as well as the respective calculated treatment cost.

Similarly, in Cases IV to VI, the H_2O_2 flow rate is fixed and the initial iron (II) concentration varies, and for each case the final aromatic compound concentration is calculated. Table 7 also lists the three H_2O_2 flow rates (Cases IV to VI) for each case and the corresponding initial iron (II) concentration to reach the *CONAMA* requirement as well as the calculated treatment cost. Note that the *CONAMA* requirement is met only in Case VI. The stoichiometric initial iron (II) concentration for this flow rate needed to reach

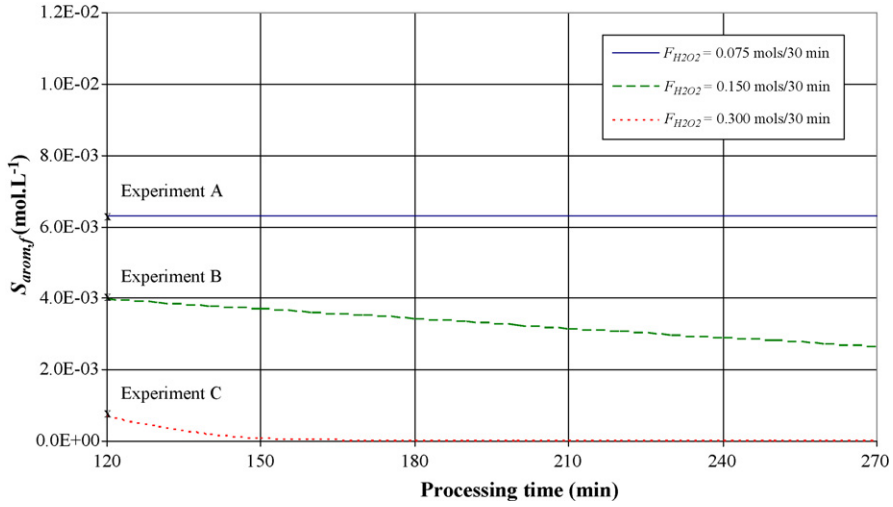

Fig. 11. Residual concentration of aromatic compounds as a function of the batch time.

Table 7
Treatment cost for phenol contaminated wastewater as a function of initial iron (II) concentration and H_2O_2 flow rate.

Case	$S_{Fe_{2+},0}$ (mol L^{-1})	$F_{H_2O_2}$ (mol/30 min)	Treatment cost (US$/1000 m^3 of wastewater)
I	0.5×10^{-3}	0.678	696
II	1.0×10^{-3}	0.367	403
III	5.0×10^{-3}	0.171	351
IV	–	0.075	Cannot meet *CONAMA's* requirement
V	–	0.150	Cannot meet *CONAMA's* requirement
VI	1.40	0.300	351

that requirement is 1.4×10^{-3} mol L^{-1}, and the corresponding calculated treatment cost is \$316/1000 m^3 of wastewater.

From the results shown in Fig. 10, the treatment cost as a function of the required residual aromatic compounds concentration, $S_{arom,f}$ is calculated. The three curves shown in Fig. 12 represent different initial iron (II) concentrations. Note that a stricter requirement for residual aromatic compounds would significantly increase operating costs.

For the three cases shown in Fig. 12, an initial iron (II) concentration of 5.0×10^{-3} mol L^{-1} yielded the lowest cost to meet *CONAMA*'s requirement for phenol.

Fig. 13 presents the treatment cost as a function of different initial phenol concentrations, $S_{phenol,0}$, that meet *CONAMA*'s requirement for the three initial iron (II) concentrations used in Fig. 10. Note that the analyzed phenol concentration values are within the ranges typically found in wastewater streams (Pryia et al. [26]).

For an initial phenol concentration of 5.0×10^{-3} mol L^{-1}, the cost for treatments with initial iron (II) concentrations of 0.5×10^{-3} and 1.0×10^{-3} mol L^{-1} are basically the same (less than 4% difference), but as the initial phenol concentration increases, the cost of the treatment with $S_{Fe_{2+},0} = 0.5 \times 10^{-3}$ mol L^{-1} presents a higher slope than the one with $S_{Fe_{2+},0} = 1.0 \times 10^{-3}$ mol L^{-1}. Similarly to Fig. 12, the treatment with $S_{Fe_{2+},0} = 5.0 \times 10^{-3}$ mol L^{-1} has the lowest cost.

Nevertheless, *CONAMA* also restricts the overall iron concentration, in both valence states, in the wastewater to a maximum value of 15.0 mg/L (0.27×10^{-3} mol L^{-1}) that is approximately half of the one used in Case I, which uses the lowest iron concentration (note that the initial and the final overall iron concentrations are

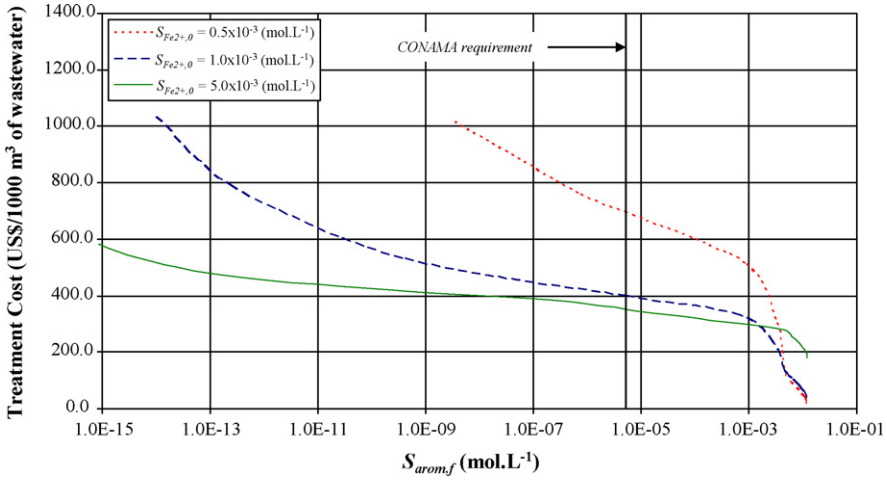

Fig. 12. Treatment cost as a function of the residual concentration of aromatic compounds.

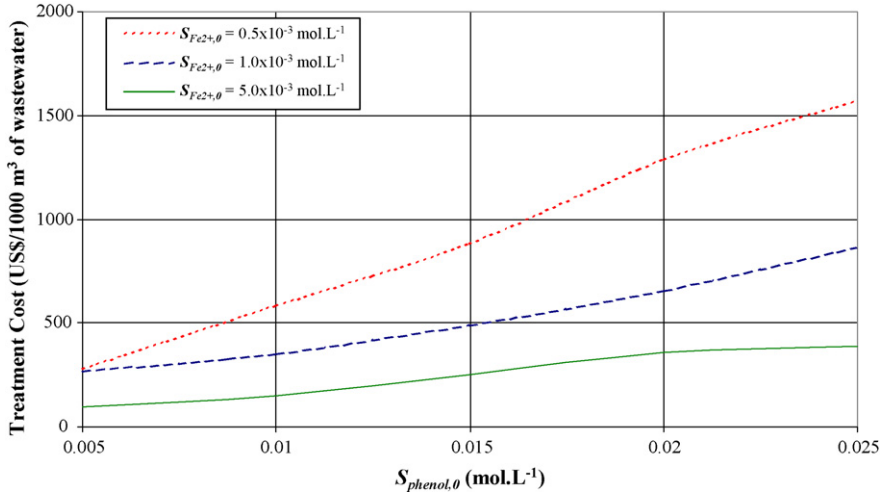

Fig. 13. Treatment cost as a function of the initial phenol concentration.

the same). The use of iron then requires additional treatment of the wastewater to remove it from the effluent. Consequently, the overall minimum cost would require the integrated analysis of the two treatment phases.

7. Conclusions

The present paper addressed the mathematical modeling of the phenol degradation by the Fenton process. First, it develops a stoichiometric model, followed by a kinetic model. The developed model encompasses 53 reactions and 26 compounds and is able to predict the oxidation of phenol in the *ortho* and *para* positions resulting in aromatic isomers that are catechol and hydroquinone.

Three experiments were performed to study the degradation of phenol by the Fenton process in fed-batch operation, monitoring the phenol, catechol and hydroquinone concentrations during 2 h.

Sensitivity analysis was performed on the kinetic parameters to determine those that are most influential in the final phenol, catechol and hydroquinone concentrations. As expected, the most influential parameters are the ones that regulate the oxidation by hydroxyl radical reactions involving these three studied compounds. Parameter estimation was performed to best fit the experimental data and the overall correlation coefficient obtained was 0.93.

Using the estimated kinetic parameters, an initial concentration analysis of the reactants was performed, showing that excess iron (II) in the reaction medium causes an efficiency loss of the Fenton process due to the competition of the iron (II) ions with the organic compounds for the hydroxyl radicals in the case of an insufficient quantity of H_2O_2 added to the reaction medium.

Finally, cost analysis was made for the treatment of the phenol contaminated wastewater used in the experiments with different initial iron (II) concentrations and H_2O_2 flow rates. It was shown that of the three H_2O_2 flow rates used in the experiments, only the one used in Experiment C (0.300 mol/30 min) was able to meet the *CONAMA* standard for maximum concentration of residual aromatic compounds. For environmental requirements stricter than *CONAMA*'s and different initial phenol concentrations, the initial iron (II) concentration used in Case III ($5\,mmol\,L^{-1}$) yields lower treatment costs than the other two cases.

Further developments include the integrated optimization of the process consisting of a Fenton reaction and iron purification, as well as the extension of the model to address photo-Fenton processes.

Acknowledgements

The authors acknowledge financial support from CAPES (Brazil).

References

[1] O. Legrini, E. Oliveros, A.M. Braun, Photochemical processes for water treatment, Chemical Reviews 93 (1993) 671–698.
[2] P.R. Gogate, A.B. Pandit, A review of imperative technologies for wastewater treatment II: hybrid methods, Advances in Environmental Technology Research 8 (2004) 553–597.
[3] M. Pera-Titus, V. García-Molina, M.A. Baños, J. Giménez, S. Esplugas, Degradation of chlorophenols by means of advanced oxidation processes: a general review, Applied Catalysis B: Environmental 47 (2004) 219–256.
[4] A. Machulek Jr., J.E.F. Moraes, C. Vautier-Giongo, C.A. Silverio, L.C. Friedrich, C.A.O. Nascimento, M.C. Gonzalez, F.H. Quina, Abatement of the inhibitory effect of chloride anions on the photo-Fenton process, Environmental Science and Technology 41 (24) (2007) 8459–8463.
[5] S. Esplugas, J. Giménez, S. Contreras, E. Pascual, M. Rodríguez, Comparison of different advanced oxidation processes for phenol degradation, Water Research 36 (2002) 1034–1042.
[6] J.E.F. Moraes, D.N. Silva, F.H. Quina, O. Chiavone-Filho, C.A.O. Nascimento, Utilization of solar energy in the photodegradation of gasoline in water and of oil-field-produced water, Environmental Science and Technology 38 (13) (2004) 3746–3751.
[7] M. Rios-Enriquez, N. Shahin, C. Durán-de-Bazúa, J. Lang, E. Oliveros, S.H. Bossmann, A.M. Braun, Optimization of the heterogeneous Fenton-oxidation of the model pollutant 2,4-xylidine using the optimal experimental design methodology, Solar Energy 77 (2004) 491–501.
[8] A.C.S.C. Teixeira, R. Guardani, C.A.O. Nascimento, Solar photochemical degradation of aminosilicones contained in liquid effluents. process studies and neural network modeling, Industrial & Engineering Chemistry Research 42 (2003) 5751–5761.
[9] J.E.F. Moraes, D.N. Silva, F.H. Quina, C.A.O. Nascimento, O. Chiavone-Filho, Treatment of saline wastewater contaminated with hydrocarbons by the photo-Fenton process, Environmental Science and Technology 38 (4) (2004) 1183–1187.
[10] J.A. Giroto, R. Guardani, A.C.S.C. Teixeira, C.A.O. Nascimento, Study on the photo-Fenton degradation of polyvinyl alcohol in aqueous solution, Chemical Engineering and Processing 45 (2006) 523–532.
[11] N. Kang, D.S. Lee, J. Yoon, Kinetic modeling of Fenton oxidation of phenol and monochlorophenols, Chemosphere 47 (2002) 915–924.
[12] H. Kusic, N. Koprivanac, A. Loncaric Bosic, I. Selenec, Photo-assisted Fenton type processes for the degradation of phenol: a kinetic study, Journal of Hazardous Materials B136 (2006) 632–644.
[13] R. Andreozzi, A. D'Apuzzo, R. Marotta, A kinetic model for the degradation of benzothiazole by Fe^{3+}-photo-assisted Fenton process in a completely mixed batch reactor, Journal of Hazardous Materials B80 (2000) 241–257.
[14] R.F.F. Pontes, J.M. Pinto, Analysis of integrated kinetic and flow models for anaerobic digesters, Chemical Engineering Journal 122 (1–2) (2006) 65–80.
[15] K.A. Hislop, J.R. Bolton, The photochemical generation of hydroxyl radicals in the UV–vis/ferrioxalate/H_2O_2 system, Environmental Science and Technology 33 (1999) 3119–3126.
[16] J.J. Pignatello, E. Oliveros, A. Mackay, Advanced oxidation processes for organic contaminant destruction based on the Fenton reaction and related chemistry, Critical Reviews in Environmental Science and Technology 36 (1) (2006) 1–84.
[17] S.M. Kim, A. Vogelpohl, Degradation of organic pollutants by the photo-Fenton-process, Chemical Engineering Technology 21 (1998) 187–191.
[18] I.B.S. Will, J.E.F. Moraes, A.C.S.C. Teixeira, R. Guardani, C.A.O. Nascimento, Photo-Fenton degradation of wastewater containing organic compounds in solar reactors, Separation and Purification Technology 34 (2004) 51–57.
[19] R. Alnaizy, A. Akgerman, Advanced oxidation of phenolic compounds, Advances in Environmental Research 4 (2000) 233–244.
[20] Notre Dame Radiation Chemistry Data Center – http://www.rcdc.nd.edu/, accessed 20-05-09.
[21] J. De Laat, G.T. Le, B. Legube, A comparative study of the effects of chloride, sulfate and nitrate ions on the rates of decomposition of H_2O_2 and organic compounds by Fe(II)/H_2O_2 and Fe(III)/H_2O_2, Chemosphere 55 (2004) 715–723.
[22] L.F. Shampine, M.W. Reichelt, J.A. Kierzenka, Solving index-1 DAEs in MATLAB and Simulink, SIAM Review 41 (1999) 538–552.
[23] T.F. Coleman, Y. Li, An interior, trust region approach for nonlinear minimization subject to bounds, SIAM Journal on Optimization 6 (1996) 418–445.
[24] E. Lipczynska-Kochany, Hydrogen peroxide mediated photodegradation of phenol as studied by a flash photolysis/HPLC technique, Environmental Pollution 80 (20) (1993) 147–152.
[25] CONAMA – Conselho Nacional do Meio Ambiente Resolution No 357, March 17, 2005 – São Paulo, Brazil.
[26] S.S. Priya, M. Premalatha, N. Anantharaman, Solar photocatalytic treatment of phenolic wastewater – potential, challenges and opportunities, ARPN Journal of Engineering and Applied Sciences 3 (6) (2008) 36–41.